ACS APPLIED MATERIALS & INTERFACES

Research Article

www.acsami.org

Synergistically Enhanced Electrochemical Response of Host–Guest Recognition Based on Ternary Nanocomposites: Reduced Graphene Oxide-Amphiphilic Pillar[5]arene-Gold Nanoparticles

Jun Zhou,[†,‡] Ming Chen,[†] Ju Xie,[†] and Guowang Diao[†,*]

[†]College of Chemistry and Chemical Engineering, Yangzhou University, Yangzhou 225002, Jiangsu, People's Republic of China

[‡]Nantong Vocational College, Nantong 226001, Jiangsu, People's Republic of China

Supporting Information

ABSTRACT: An amphiphilic pillar[5]arene (AP5) was modified onto the surface of reduced graphene oxide (RGO) to form the water-dispersive RGO-AP5 nanocomposite. And then, as-prepared gold nanoparticles (AuNPs) self-assembled onto the surface of RGO-AP5 through amido groups of AP5 to achieve RGO-AP5-AuNPs nanocomposites. It was verified that a large amount of AP5 molecules had been effectively loaded onto the surface of RGO and lots of AuNPs could be uniformly dispersed on RGO-AP5. Electrochemical results showed that the RGO-AP5 could exhibit selective supramolecular recognition and enrichment capability toward guest molecules. More significantly, in electrochemical sensing the guest molecules, ternary nanocomposites RGO-AP5-AuNPs performed the synergetic action of multifunctional properties, which were excellent performances of RGO, selective supramolecular recognition, and enrichment capability of AP5 and catalytic property of AuNPs for guest molecules. Therefore, RGO-AP5-AuNPs showed an outstanding analyzing performance for DA with broad linear range (1.5×10^{-8} to 1.9×10^{-5} M) and low detection limit (1.2×10^{-8} M) at a signal-to-noise ratio of 3.

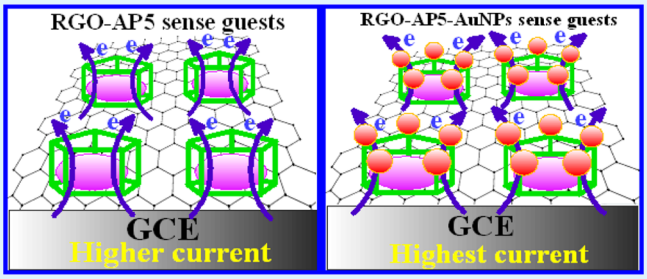

KEYWORDS: *reduced graphene oxide, pillar[5]arene, gold nanoparticles, host–guest recognition, synergetic action*

1. INTRODUCTION

The arrival of any new generation of macrocycle hosts with fascinating properties can accelerate the development of supramolecular chemistry and pave a new way for materials science. These macrocycles, such as crown ethers,[1,2] cyclodextrins,[3,4] cucurbiturils,[5,6] calixarenes,[7,8] have attracted much interest because of their applications in a broad range of fields.[9−15] Within the last 5 years, as a new class of supramolecular hosts, pillar[n]arenes, especially pillar[5]arenes, because of unique structures and intriguing properties, have been actively studied and rapidly developed. Pillar[n]arenes consist of hydroquinone units linked by methylene bridges at para positions and meanwhile possess a hydrophobic core sandwiched between two functionalizable rims. Therefore, the structure of pillar[n]arene is a rigid symmetrical pillar architecture and differ from the flexible vase-shape architecture of meta-bridged calixarenes. Because of their rigid pillar architecture and hydrophobic electron-donating cavities, pillar[n]arenes have displayed unique binding abilities to various guest molecules and exhibited attractive properties during the process of application such as nanomaterials, molecular recognition, chemosensors, ion transport, supramolecular polymers.[16−35] Recently, an amphiphilic pillar[5]arene (AP5) with five amino groups as the hydrophilic head and five alkyl chains as the hydrophobic tail was designed and synthesized.[36] Figure 1B displays the molecular structure of AP5. AP5 contains not only one hydrophobic cavity but also five hydrophilic amino groups, which can absorb noble metal nanoparticles to produce multifunctional nanocomposites with potential applications in materials science.

Graphene has attracted considerable scientific interest because of its remarkable mechanical properties, high surface area, and fascinating electronic transfer.[37−39] The reduced graphene oxide (RGO), achieved by means of chemical reduction of graphene oxide (GO), has a comparatively lower conductivity compared with the mechanically cleaved graphene, but is still a versatile material. Therefore, RGO is an ideal building block in nanocomposites. Over the past few years, RGO-metal-nanoparticles nanocomposites (possessing excellent performances of RGO and catalytic properties of metal-nanoparticle) have been intensively developed and used as the electrocatalysts to improve the detection sensitivity of analytes.[40−43] Up to now, RGO-metal-nanoparticle nanocomposites have been prepared through two different ways, including in situ growth[44−46] and self-assembly.[47−50] Self-assembly is a very effective strategy for fabricating RGO-metal-nanoparticle hybrid materials, where certain linkers modified on RGO can bind metal nanoparticles to RGO planes. At present,

Received: August 17, 2013
Accepted: October 3, 2013
Published: October 3, 2013

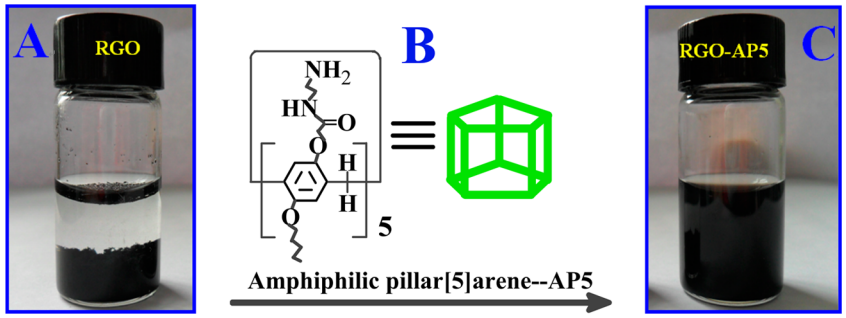

Figure 1. (A) Photo of RGO in aqueous media. (B) Chemical structure of an amphiphilic pillar[5]arene [AP5]. (C) Photo of RGO-AP5 composites in aqueous media.

various types of linker have emerged. However, some of the linkers, such as decylpyrene[49] and octadecylamine,[50] have poor water-solubility. So, the preparation and application of RGO-metal-nanoparticles are only in organic solvents such as toluene, dichloromethane, etc., which often cause environment pollution. Some linkers have good water-solubility, although in most cases, it may lead to undesirable poor performance of RGO-metal-nanoparticles in the application process. Thus, it is eagerly expected that some kinds of proper molecules, used as the linker between RGO and metal nanoparticles, can not only effectively improve water dispersibility of RGO but also synergistically enhance functions for RGO or RGO-metal-nanoparticles in many technological applications such as electrocatalysis.

Herein, we report that AP5 self-assembled onto the surface of GO (Scheme 1A) and was reduced by hydrazine to prepare water-dispersive RGO-AP5 nanocomposites (Scheme 1B). Images A and C in Figure 1 showed photos of RGO and RGO-AP5 in aqueous media. Then, assembling Au nanoparticles (AuNPs) onto RGO-AP5 fabricated RGO-AP5-AuNPs nanocomposites (Scheme 1C). Lastly, RGO (Scheme 1D), RGO-AP5 (Scheme 1E), and RGO-AP5-AuNPs (Scheme 1F) were coated onto the glassy carbon electrode (GCE) to sense guest molecules by cyclic voltammetry, and cyclic voltammograms (CVs) of these nanomaterials modified GCE showed different peak currents separately.

Scheme 1. Schematic Diagram of (A) RGO, (B) RGO-AP5, and (C) RGO-AP5-AuNPs Sensing the Guest Molecule by Cyclic Voltammetry

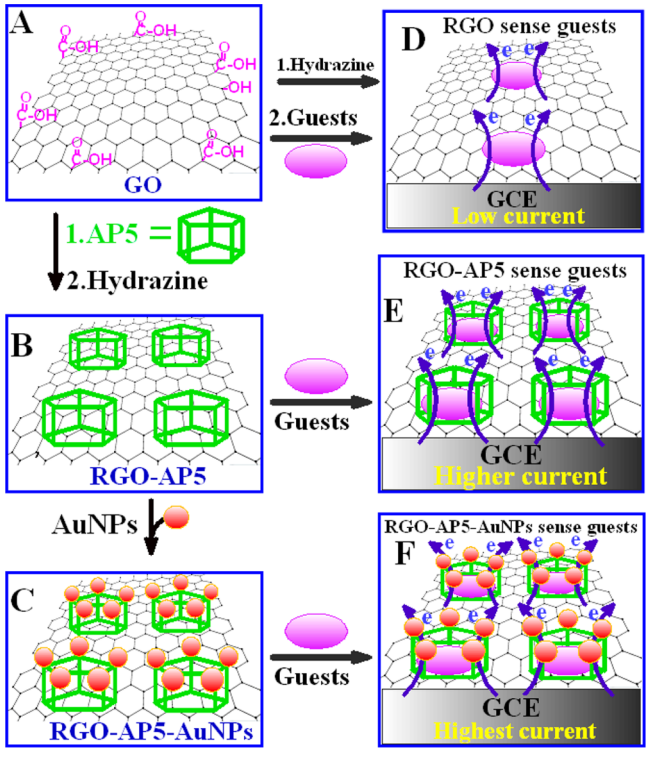

2. EXPERIMENTAL SECTION

2.1. Synthesis of RGO-AP5, RGO-AP5-AuNPs. The synthesis process of RGO-AP5 and RGO-AP5-AuNPs are as follows: Firstly, GO was prepared from natural graphite powder by Hummer's method,[51] and AP5 was synthesized according to the report.[36] GO was modified by AP5 to form GO-AP5 in water. In a typical procedure, GO (20 mg) and AP5 (20 mg) were dispersed in deionized water (20 ml) by bath-sonicating, and the mixture was allowed to stir for 12 h at room temperature. Then, after adding hydrazine hydrate (200 μL) and ammonia solution (400 μL), the mixture was stirred vigorously at 75 °C for 14 h. The black dispersion was separated by centrifuging at a speed of 10000 rpm for 20 min, then, washed with doubly distilled water three times to obtain RGO-AP5 that can be easily dispersed in water by ultrasonication again. Lastly, after AuNPs being synthesized according to report,[52] RGO-AP5 (10 mg) was added to the excess as-prepared AuNPs under vigorous stirring and the mixture was ultrasonicated for 5 min. After stirring for an additional 10 h, RGO-AP5-AuNPs were separated by centrifuging at a speed of 10 000 rpm for 10 min, washed with deionized water three times, and then dried for 2 days in a vacuum drying oven at 65 °C. Besides, the preparation of RGO was similar to RGO-AP5 composite except there was no addition of AP5.

2.2. Preparation of Modified Electrodes. The glassy carbon electrode (GCE) were polished with 0.3 μm Al_2O_3 powders and carefully cleaned with deionized water. The suspensions of RGO-AP5-AuNPs, RGO-AP5 and RGO (1 mg mL^{-1}) were prepared by dispersing RGO-AP5-AuNPs, RGO-AP5 and RGO in deionized water. The suspensions (10 μL) were dropped onto the GCE and these modified electrodes were dried in air. Finally, these modified electrodes were activated by several sequential scans with a scan rate of 100 mV s^{-1} in 0.1 M PBS (pH 7.0).

2.3. Materials Characterization. Fourier Transform infrared (FT-IR) spectra for the different samples were recorded on a Bruker Tensor 27. UV−vis spectroscopy (UV-vis) for the various samples was measured on a UV-2550 PC UV-visible spectrometer (Shimadzu, Japan). Carefully weighed quantities of every sample was subjected to TGA on a STA409PC (NETZSCH) TGA instrument at a heating rate of 10 °C·min^{-1} under vacuum from 30 to 600 °C. Transmission electron microscopy (TEM) observation was performed on a Philips TECNAI-12 instrument. X-ray Powder Diffraction (XRD) data were obtained with a graphite monochromator and Cu Kα radiation (λ = 0.1541 nm) on a D8 advance superspeed powder diffractometer (Bruker). Every electrochemical experiment was measured with a CHI660c electrochemical workstation (Chenghua, China) with a

three-electrode system including a GCE (diameter = 3 mm) as the working electrodes, a saturated calomel electrode (SCE) as the reference electrode and a Pt wire electrode as the counter electrode.

3. RESULTS AND DISCUSSION

3.1. Characterization of GO-AP5, RGO-AP5. FT-IR spectra of GO, GO-AP5, RGO-AP5, and AP5 are shown in Figure 2. By comparing these spectra, two significant features

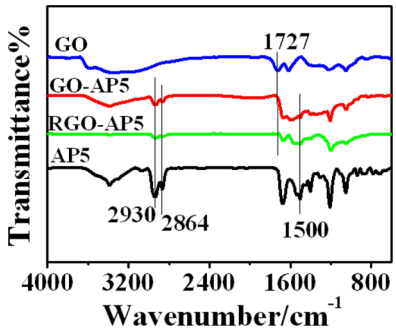

Figure 2. FT-IR spectra of GO, GO-AP5, RGO-AP5, and AP5.

can be observed: first, after GO was modified by AP5, the relative intensity of carboxylic acid −C═O stretching bands at 1727 cm^{-1} in GO-AP5 and RGO-AP5 remarkably decreases relative to GO, which may be interpreted as evidence that carboxylic acid groups interact with amine groups.[53] Second, as for GO-AP5 and RGO-AP5, the bands observed at 2930 and 2864 cm^{-1} are assigned to CH_2 asymmetric and symmetric stretching vibrations, respectively, and the bands observed at 1500 cm^{-1} are assigned to the phenyl plane bending vibrations, which indicates that AP5 molecules have been introduced to the surfaces of GO and RGO.

The successful preparation of RGO-AP5 nanocomposites is confirmed by UV-vis absorption spectra. As shown in Figure 3,

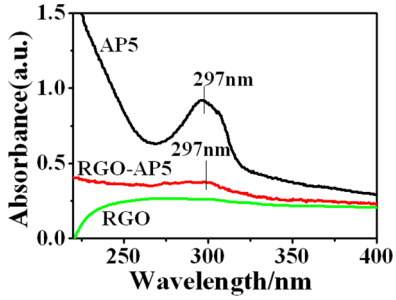

Figure 3. UV−vis spectra of RGO, RGO-AP5, and AP5.

the UV−vis spectra of pure AP5 shows a peak at about 297 nm. After AP5 was loaded onto RGO, it is found that the absorbance peak of AP5 in RGO-AP5 was also showed a weak peak at about 297 nm, which indicate that AP5 have been adsorbed onto RGO. Nevertheless, appropriate peaks do not observe from RGO. The result confirms that AP5 molecules have been successfully modified on the surface of RGO.

Thermal gravimetric analysis (TGA) was used to measure the amount of AP5 molecules on the surface of RGO. The weight losses of RGO, RGO-AP5 and AP5 are displayed in Figure 4. Pure AP5 slowly decomposed at approximately 330 °C. RGO shows much higher thermal stability with only a mass loss of 4.6% up to 600 °C. As for RGO-AP5, deducted mass

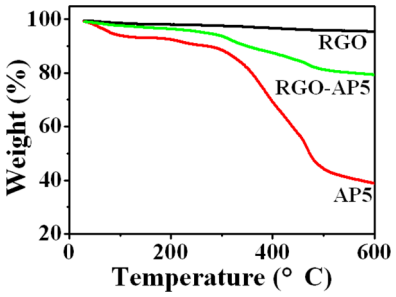

Figure 4. TGA of RGO, RGO-AP5, and AP5.

loss of RGO, the weight loss being attributed to the decomposition of AP5 is 16.3%, indicating that the amount of AP5 molecules functionalized on the surface of RGO is 16.3%. This is an exciting result because RGO loading plentiful AP5 molecules will provide a good opportunity to expand not only the supramolecular recognition and enrichment ability but also the capacity of binding AuNPs.

The self-assembly mechanism of AP5 on the surface of GO is similar to the resorcinarene,[54] and also mainly contribute to covalent bond force and non-covalent bond force. On the one hand, AP5 molecules with amino groups may react with carboxyl groups of GO to form amido bond. This has been confirmed by FT-IR spectra (Figure 2). The result shows that the covalent bond force exists between AP5 and GO. On the other hand, $\pi-\pi$ noncovalent interaction between benzene rings of calixarenes and the surface of GO (RGO) has been clarified in our previous researches.[54,55] Because of the construction of AP5 being similar to the resorcinarene, we therefore deduce that $\pi-\pi$ interaction should exist between benzene rings of AP5 and the surface of GO (RGO).

3.2. Self-Assembly of AuNPs on RGO-AP5. The immobilized AP5 on the surface of RGO were used as linker to adhere AuNPs and form RGO-AP5-AuNPs composites. Figure 5A showed the morphology of RGO-AP5-AuNPs with

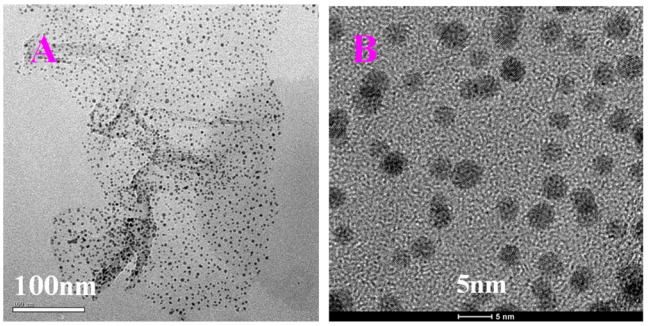

Figure 5. (A) TEM image of RGO-AP5-AuNPs with $\gamma_{A/R}$ of 1.0. (B) HRTEM image of RGO-AP5-AuNPs.

weight ratio of AP5/RGO ($\gamma_{A/R}$ = 1.0). It is clear that AuNPs on the surface of RGO were very uniform. The HRTEM image (Figure 5B) showed that the diameter of AuNPs is about 3 nm.

Figure 6 shows XRD patterns of RGO, AP5 and RGO-AP5-AuNPs with 3 nm AuNPs. For RGO, there is a broad diffraction peaks at about 24.7°. Pure AP5 powder displays a typical noncrystal diffraction at 21.7°. As for RGO-AP5-AuNPs, the diffraction peaks at 2θ = 38.4, 44.0, 64.9, and 77.9° are assigned to the Au(111), Au(200), Au(220) and Au(311), respectively. The diffraction peak at 23.5° should be the superposition diffraction peak of AP5 and RGO.

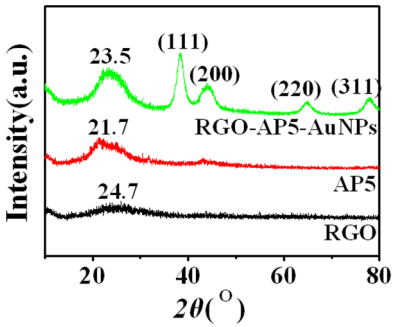

Figure 6. XRD patterns for RGO, AP5, and RGO-AP5-AuNPs.

3.3. Host−Guest Electrochemical Recognition of RGO-AP5, RGO-AP5-AuNPs. To investigate the host−guest recognition abilities of RGO-AP5 and RGO-AP5-AuNPs modified electrodes, the electrochemical behaviors were measured for six electroactive guest molecules [dopamine (DA), 4-acetamidophenol (APAP), uric acid (UA), methylene blue (MB), tryptophan (Trp), and imidacloprid (IDP)]. CVs and peak currents of six guests on (a) GCE, (b) RGO/GCE, (c) RGO-AP5/GCE, (d) RGO-AP5-AuNPs/GCE were shown in Figure 7A−F and G−L, respectively.

On bare GCE, there were very weak anodic or cathodic peaks for six guests, as shown in Figure 7A-F (curve a). Meanwhile, on RGO/GCE, the peak currents for six guests had a visible increase (Figure 7A−F, curve b), which was mainly due to excellent conductivity and large surface area of RGO.

Interestingly enough, on RGO-AP5/GCE, because of AP5 being introduced into RGO, there was markedly different electrochemical response for six different guests. The peak currents for the first four kinds of guests (DA, APAP, UA, MB) were enhanced and were approximately 1.3-2.5 times as much as those on RGO/GCE, which should be attributed to the host−guest recognition and enrichment effect between AP5 and the guests. However, for Trp, the peak current on RGO-AP5/GCE was almost unchanged (Figure 7E, curve c). As for IDP, no cathodic peak can be observed on RGO-AP5/GCE (Figure 7F, curve c). For comparison's sake, the current densities on RGO/GCE and RGO-AP5/GCE for six guest molecules were detailed in Table 1.

On the basis of the above experiential phenomena, obviously, because of modifying AP5 (hosts) on the surface of RGO, there were markedly different enrichment effects and electrochemical response for six different guests on RGO-AP5/GCE. This result can be expounded from two aspects: On the one hand, dimensions of guest molecules may mainly affect their enrichment effect on RGO-AP5/GCE. Generally speaking, the principle of dimension matching is one of important factors to influence the formation of host−guest inclusion complexes. Pillar[5]arene has a rigid hydrophobic cavity. The cavity depth of pillar[5]arene is about 7.8 Å and the diameter is about 5.6 Å,[56] just like the sizes in Figure 8. One dimension sizes of DA (4.5 Å), APAP (4.9 Å), UA (5.1 Å), and MB (5.2 Å) are smaller than the diameter of pillar[5]arene, as shown in Figure 9. So, four guest molecules can easily enter the cavity of AP5 to form inclusion complexes, which makes it possible to accumulate above guests onto the surface of RGO-AP5/GCE and accordingly improve the electrochemical response. However, if larger molecules, for example, Trp (one dimension size, 5.5 Å, which is near to the diameter of the cavity of AP5) or IDP (one dimension size, 6 Å, which is larger than the diameter of cavity

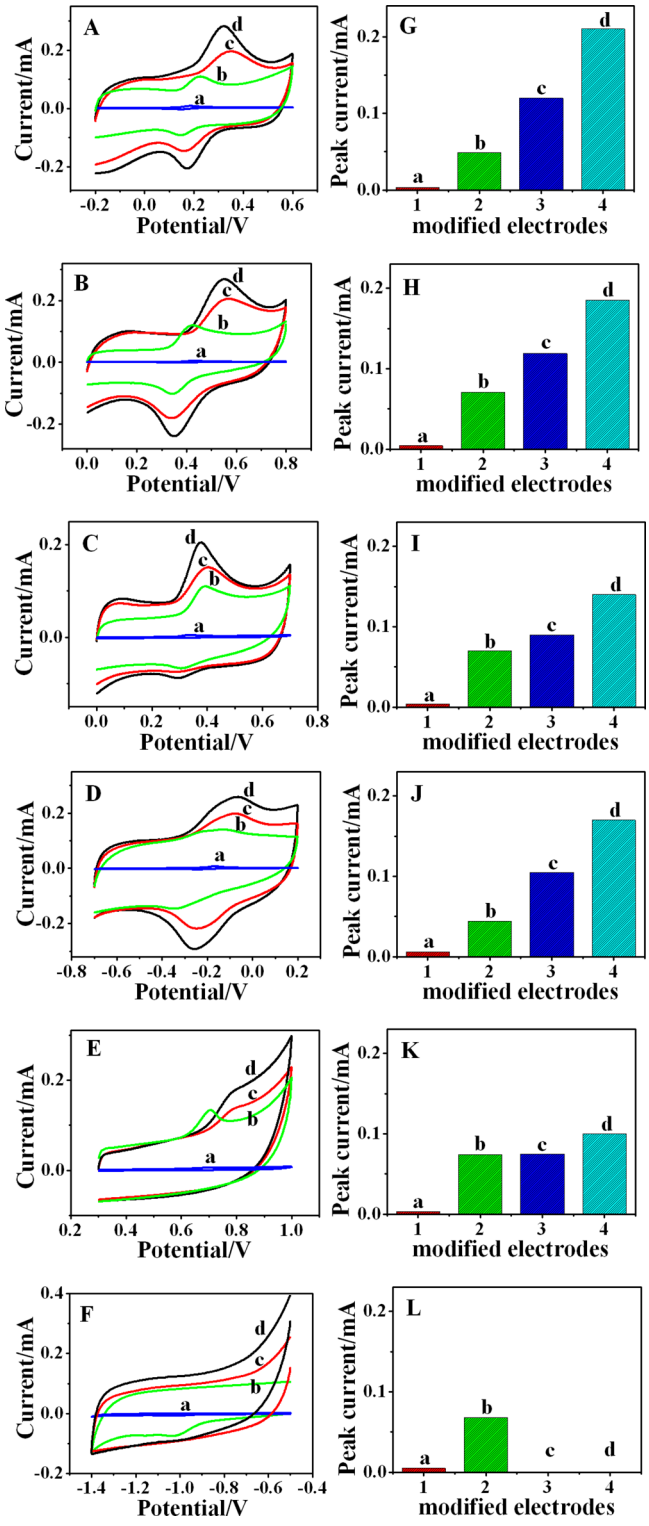

Figure 7. CVs and peak current of CVs of (A, G) 50 μM DA, (B, H) 50 μM APAP, (C, I) 50 μM UA, (D, J) 50 μM MB, (E, K) 50 μM Trp, and (F, L) 50 μM IDP in 0.1 M phosphate buffer (pH 7) on (a) bare GCE, (b) RGO/GCE, (c) RGO-AP5/GCE, (d) RGO-AP5-AuNPs/GCE.

of AP5, Figure 10) were selected as guests, the electrochemical behaviors of them were shown in panels E and F in Figure 7. According to curves b and c in Figure 7E, the peak current was almost same before and after the modification of AP5 onto RGO/GCE, which indicated that the interaction between AP5

dx.doi.org/10.1021/am403463p | ACS Appl. Mater. Interfaces 2013, 5, 11218−11224

Table 1. Current Densities of CVs of 50 μM DA, APAP, UA, MB, Trp, IDP in 0.1 M Phosphate Buffer (pH 7) on RGO/GCE, RGO-AP5/GCE, RGO-AP5-AuNPs/GCE

	current densities(mA mM^{-1} L cm^{-2})		
guest molecules	RGO/GCE	RGO-AP5/GCE	RGO-AP5-AuNPs/GCE
DA	14.2 ± 0.14	33.6 ± 0.2	60.3 ± 0.34
APAP	19.8 ± 0.12	33.2± 0.2	56.9± 0.28
UA	19.8 ± 0.25	24.7 ± 0.18	39.2 ± 0.20
MB	12.5 ± 0.12	30.2 ± 0.15	49.6 ± 0.15
Trp	20.9 ± 0.20	21.2 ± 0.13	28.3 ± 0.15
IDP	19.3 ± 0.10	0	0

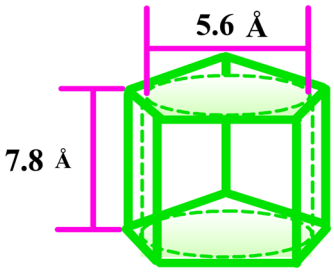

Figure 8. Structure and two dimension sizes of pillar[5]arene.[56]

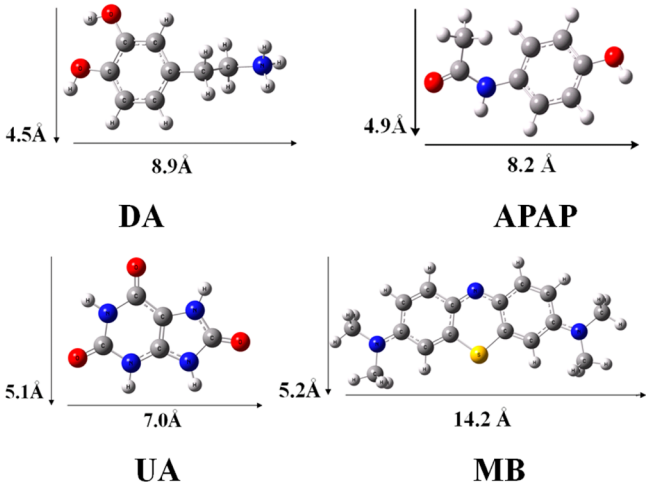

Figure 9. Molecular models of DA,[55] APAP, UA[55], and MB[55] and calculated dimensions. The structures were predicted by DFT method using Gaussian 09.

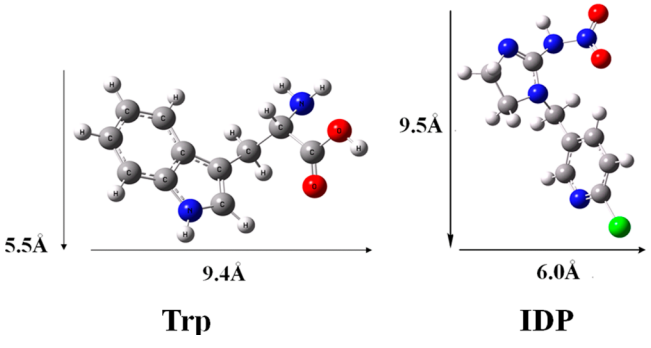

Figure 10. Molecular models of Trp and [55] IDP and calculated dimensions. The structures were predicted by DFT method using Gaussian 09.

and Trp was very weak. The weak interaction between AP5 and Trp may be attributed to the closed dimensions of both host cavity and guest so that the guest was difficult to enter into the cavity of AP5. Furthermore, if IDP, whose size is larger than the diameter of the cavity of AP5, was selected as electroactive species, IDP cannot enter into the cavity of AP5, which would prevent IDP from approaching the RGO layer on the electrode and accordingly no cathodic peak can be observed on RGO-AP5/GCE (Figure 7F, curve c). Therefore, AP5 will strictly perform the rule of dimension matching and selectively include guest molecules during the molecular recognition process, which is markedly different with calixarenes. Calixarenes possessing relatively flexible structures may form inclusion complexes with some guest molecules whose one dimension sizes are smaller, close to or slightly larger than the diameter of calixarenes.[55,57−60] On the other hand, charge properties of guest molecules may affect the enrichment effect of RGO-AP5/GCE. The electron-donating cavity of AP5 easily forms inclusion complexes with various electron-deficient guests or neutral molecules being small enough to fit into their cavities.[25] Among the first four investigated molecules, DA and MB have positive charges and APAP is neutral molecule. So, three guest molecules can easily form inclusion complexes with AP5. Correspondingly, DA, APAP, and MB on RGO-AP5/GCE showed relatively high current densities. On the contrary, UA with negative charges on RGO-AP5/GCE showed relatively low current densities. Therefore, except for dimensions of guest molecules, charge properties of guest molecules will also affect their enrichment effect on RGO-AP5/GCE. In brief, the synergy of two factors may lead to different inclusion constants between substrates (DA, APAP, UA, MB,Trp, IDP) and AP5 (see Table S1 in the Supporting Information). For this reason, six guests on RGO-AP5/GCE showed remarkably different electrochemical response.

More interestingly, because of AuNPs being introduced onto the surface of RGO-AP5, for guest molecules with the matching dimension of AP5, such as DA, APAP, UA, and MB, the peak currents achieved a further increase and were about 2-fold as much as those on RGO-AP5/GCE, as shown in Figure 7A−D (curve d). The effect of the scanning rate (ν) on the peak current of DA has also been investigated by CV method (see Figure S1A in the Supporting Information). It is obvious that the anodic peak currents (I_{pa}) were affected by scan rate at the range of 10−180 mV s^{-1}. Figure S1B in the Supporting Information showed that the anodic currents were linear with the square root of the scan rate, indicating that the system presents a diffusion-controlled process of DA on the surface of RGO-AP5-AuNPs/GCE in the studied range of potential sweep rates. Meanwhile, RGO-AP5-AuNPs/GCE for four guests also showed highest current densities in three kinds of modified electrodes (Table 1). In addition, the anodic peak potentials of four guests on RGO-AP5-AuNPs/GCE have negative shift compared with those of RGO-AP5/GCE (DA: moving from 0.35 to 0.32 V; APAP, moving from 0.57 to 0.54 V; UA, moving from 0.40 to 0.38 V; MB, moving from −0.075 to −0.077 V). However, because of the weak interaction between AP5 and Trp, the peak current of Trp on RGO-AP5-AuNPs/GCE obtained a slight increase and was only about 1.3-fold as much as that on RGO-AP5/GCE (Figure 7E, curves c and d). Furthermore, because AP5 cannot recognize IDP, just like on RGO-AP5/GCE, no cathodic peak can be observed on RGO-AP5-AuNPs/GCE (Figure 7F, curve d). Given the above, AuNPs capping on the surface of RGO-AP5 exhibit the

excellent electrocatalysis property and further accelerate the electron transfer performance between the modifying layer and the guest molecules, as is shown in Scheme 1. Thus, in the process of the host−guest electrochemical recognition, ternary nanocomposites RGO-AP5-AuNPs performed the synergetic action of multifunctional properties, which exhibited excellent conductivity and large surface area of RGO, selective supramolecular recognition and enrichment capability of AP5, and catalytic property of AuNPs for four guests.

No doubt, RGO-AP5-AuNPs are excellent electrode materials for selectively improving the electrochemical response for guests. Lots of literatures have reported that composites of macrocycle hosts can be applied to the electrochemical analysis because of host−guest inclusion interactions.[55,61−63] Here, to further investigate the sensing performance of RGO-AP5-AuNPs toward certain guest molecules, RGO-AP5-AuNPs were used to modify GCE to detect DA electrochemically using the differential pulse voltammetry (DPV). Figure 11A shows DPV

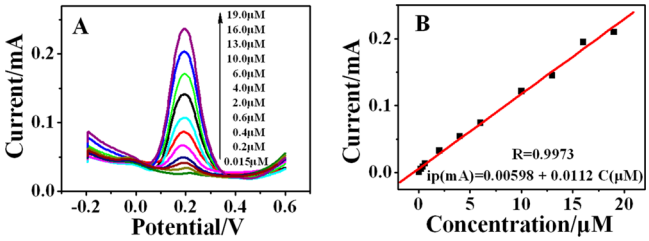

Figure 11. (A) DPV response for the different concentrations of DA on RGO-AP5-AuNPs/GCE in 0.1 M PBS (pH 7). (B) The calibration curve of DA.

response for different concentrations of DA, and a linear relationship between oxidation current and DA concentration was obtained in the range of 1.5 $\times 10^{-8}$ to 1.9$\times 10^{-5}$ mol L^{-1} (Figure 11B). The linear regression equation is defined as i (mA) = 0.00598 + 0.0112 C_{DA} (μM) with a correlation coefficient of R = 0.9973, and lowest detection limit was evaluated to be 1.2$\times 10^{-8}$ mol L^{-1} (S/N = 3). This value is much better than those of recent state-of-art binary carbon-based nanocomposites for DA reported previously for the Table 2,[43,63−67] which indicates that the RGO-AP5-AuNPs exhibit very high electrochemical analyzing performance toward the target molecules. The reason is that the synergetic action of ternary nanocomposites RGO-AP5-AuNPs improves the detecting sensitivity and reduces detection limit in electrochemical sensing the guest molecules.

Table 2. Comparison of Analytical Performance of Some Modified Electrodes for the Determination of DA

modified electrodes	linear range/ DPV	detection limit	ref
Pt/graphene nanocomposite/GCE	0.03−8.13 μM	0.03 μM	43
CD-graphene/GCE	0.1−18 μM	20 nM	63
Pt nanoparticles decorated the multiwall carbon nanotube/GCE	0.043−62 μM	0.028 μM	64
palladium nanoparticle-loaded carbon nanofibers modified carbon paste electrode	0.5−160 μM	0.2 μM	65
chitosan-graphene/GCE	1.0−24 mM	1.0 mM	66
β-CD-multiwall carbon nanotubes/ GCE	0.01−0.08 mM	37 μM	67
RGO-AP5-AuNPs/GCE	0.015−19 μM	0.012 μM	this work

4. CONCLUSION

We have developed a facile and rapid method for the synthesis of water-dispersive RGO-AP5 and extremely versatile RGO-AP5-AuNPs hybrid nanomaterials by highly efficient self-assembly method. RGO-AP5/GCE showed selective supramolecular recognition and enrichment capability and consequently displayed high electrochemical response toward guest molecules with the matching dimension of AP5, which indicates that RGO-AP5 possesses simultaneously good properties of RGO and unique natures of the rigid pillar structures and electron-donating cavities of AP5. More importantly, in the process of the host−guest electrochemical recognition, ternary nanocomposites RGO-AP5-AuNPs could exert their respective superiorities, including excellent conductivity and large surface area of RGO, selective supramolecular recognition and enrichment capability of AP5, and catalytic property of AuNPs to enhance the electrochemical response for the guests. Thus, RGO-AP5-AuNPs exhibited an excellent electrochemical analyzing performance for DA with broad linear range (1.5 $\times$ 10^{-8} to 1.9 $\times$ 10^{-5} M) and very low detection limit (1.2 $\times$ 10^{-8} M) at a signal-to-noise ratio of 3. This research is very significant not only because it expands the application of pillar[n]arene but also because it provides a new universal idea for fabricating other ternary nanocomposites RGO-macrocycle-metal naparticles that can synergistically enhance certain functions for many technological applications.

■ ASSOCIATED CONTENT

Ⓢ Supporting Information

The effect of the scanning rate (ν) on the peak current of DA on RGO-AP5-AuNPs/GCE. The inclusion constants between substrates (DA, APAP, UA, MB, Trp, IDP) and AP5. This material is available free of charge via the Internet at http://pubs.acs.org.

■ AUTHOR INFORMATION

Corresponding Author

*E-mail: gwdiao@yzu.edu.cn.

Notes

The authors declare no competing financial interest.

■ ACKNOWLEDGMENTS

This work was financially supported by the National Natural Science Foundation of China (Grant 20973151, 20901065, and 21273195), a Project Funded by the Priority Academic Program Development of Jiangsu Higher Education Institutions. This work was also financially supported by an applied research plan (Grant BK2013016).

■ REFERENCES

(1) Krakowiak, K. E.; Bradshaw, J. S.; Zamecka-Krakowiak, D. J. *Chem. Rev.* **1989**, *89*, 929−972.
(2) Gokel, G.W.; Leevy, W. M.; Weber, M. E. *Chem. Rev.* **2004**, *104*, 2723−2750.
(3) Harada, A.; Hashidzume, A.; Yamaguchi, H.; Takashima, Y. *Chem. Rev.* **2009**, *109*, 5974−6023.
(4) Liao, X. J.; Chen, G. S.; Liu, X. X.; Chen, W. X.; Chen, F. E.; Jiang, M. *Angew. Chem., Int. Ed.* **2010**, *49*, 4409−4413.
(5) Bhasikuttan, A. C.; Pal, H.; Mohanty, J. *Chem. Commun.* **2011**, *47*, 9959−9971.

(6) Jeon, Y. J.; Kim, H.; Jon, S.; Selvapalam, N.; Seo, D. H.; Oh, I.; Park, C. S.; Jung, S. R.; Koh, D. S.; Kim, K. J. *Am. Chem. Soc.* **2004**, *126*, 15944−15945.
(7) Botana, E.; Da Silva, E.; Benet-Buchholz, J.; Ballester, P.; de Mendoza, J. *Angew. Chem., Int. Ed.* **2007**, *46*, 198−201.
(8) Philip, I. E.; Kaifer, A. E. *J. Am. Chem. Soc.* **2002**, *124*, 12678−12679.
(9) Sauvage, J. P. *Acc. Chem. Res.* **1998**, *31*, 611−619.
(10) Huang, F.; Fronczek, F. R.; Gibson, H. W. A. *J. Am. Chem. Soc.* **2003**, *125*, 9272−9273.
(11) Huang, F.; Gibson, H. W. *J. Am.Chem. Soc.* **2004**, *126*, 14738−14739.
(12) Kay, E. R.; Leigh, D. A.; Zerbetto, F. *Angew. Chem., Int. Ed.* **2006**, *46*, 72−191.
(13) Shen, M.; Sun, Y.; Han, Y.; Yao, R.; Yan, C. *Langmuir* **2008**, *24*, 13161−13167.
(14) Sun, Y.; Yao, Y.; Yan, C. G.; Han, Y.; Shen, M. *ACS Nano* **2010**, *4*, 2129−2141.
(15) Sun, Y.; Yan, C. G.; Yao, Y.; Han, Y.; Shen, M. *Adv. Funct. Mater.* **2008**, *18*, 1−10.
(16) Ogoshi, T.; Kanai, S.; Fujinami, S.; Yamagishi, T. A.; Nakamoto, Y. *J. Am. Chem. Soc.* **2008**, *130*, 5022−5023.
(17) Han, C.; Yu, G.; Zheng, B.; Huang, F. *Org. Lett.* **2012**, *14*, 1712−1715.
(18) Cao, D.; Kou, Y.; Liang, J.; Chen, Z.; Wang, L.; Meier, H. *Angew. Chem., Int. Ed.* **2009**, *48*, 9721−9723.
(19) Ogoshi, T.; Hashizume, M.; Yamagishi, T.; Nakamoto, Y. *Chem. Commun.* **2010**, *46*, 3708−3710.
(20) Zhang, Z.; Yu, G.; Han, C.; Liu, J.; Ding, X.; Yu, Y.; Huang, F. *Org. Lett.* **2011**, *13*, 4818−4821.
(21) Zhang, Z.; Luo, Y.; Chen, J.; Dong, S.; Yu, Y.; Ma, Z.; Huang, F. *Angew. Chem., Int. Ed.* **2011**, *50*, 1397−1401.
(22) Strutt, N. L.; Forgan, R. S.; Spruell, J. M.; Botros, Y. Y.; Stoddart, J. F. *J. Am. Chem. Soc.* **2011**, *133*, 5668−5671.
(23) Si, W.; Chen, L.; Hu, X. B.; Tang, G.; Chen, Z.; Hou, J. L.; Li, Z. T. *Angew. Chem., Int. Ed.* **2011**, *50*, 12564−12568.
(24) Li, C.; Shu, X.; Li, J.; Chen, S.; Han, K.; Xu, M.; Hu, B.; Yu, Y.; Jia, X. *J. Org. Chem.* **2011**, *76*, 8458−8465.
(25) Xue, M.; Yang, Y.; Chi, X.; Zhang, Z.; Huang, F. *Acc. Chem. Res.* **2012**, *45*, 1294−1308.
(26) Yu, G.; Han, C.; Zhang, Z.; Chen, J.; Yan, X.; Zheng, B.; Liu, S.; Huang, F. *J. Am. Chem. Soc.* **2012**, *134*, 8711−8717.
(27) Ma, Y.; Chi, X.; Yan, X.; Liu, J.; Yao, Y.; Chen, W.; Hou, J. L.; Huang, F. *Org. Lett.* **2012**, *14*, 1532−1535.
(28) Zhang, Z.; Han, C.; Yu, G.; Huang, F. *Chem. Sci.* **2012**, *3*, 3026−3031.
(29) Cragg, P. J.; Sharma, K. *Chem. Soc. Rev.* **2012**, *41*, 597−607.
(30) Yu, G.; Zhou, X.; Zhang, Z.; Han, C.; Mao, Z.; Gao, C.; Huang, F. *J. Am. Chem. Soc.* **2012**, *134*, 19489−19497.
(31) Wei, P.; Yan, X.; Li, J.; Ma, Y.; Huang, F. *Chem. Commun.* **2013**, *49*, 1070−1072.
(32) Yao, Y.; Xue, M.; Chi, X.; Ma, Y.; He, J.; Abliz, Z.; Huang, F. *Chem. Commun.* **2012**, *48*, 6505−6507.
(33) Gao, L.; Zheng, B.; Yao, Y.; Huang, F. *Soft Matter* **2013**, *9*, 7314−7319.
(34) Yao, Y.; Xue, M.; Zhang, Z.; Zhang, M.; Wang, Y.; Huang, F. *Chem. Sci.* **2013**, *4*, 3667−3672.
(35) Yu, G.; Ma, Y.; Han, C.; Yao, Y.; Tang, G.; Mao, Z.; Gao, C.; Huang, F. *J. Am. Chem. Soc.* **2013**, *135*, 10310−10313.
(36) Yao, Y.; Xue, M.; Chen, J.; Zhang, M.; Huang, F. *J. Am. Chem. Soc.* **2012**, *134*, 15712−15715.
(37) Lee, C.; Wei, X. D.; Kysar, J. W.; Hone, J. *Science* **2008**, *321*, 385−388.
(38) Stoller, M. D.; Park, S. J.; Zhu, Y. W.; An, J. H.; Ruoff, R. S. *Nano Lett.* **2008**, *8*, 3498−3502.
(39) Service, R. F. *Science* **2008**, *322*, 1785−1785.
(40) Bai, H.; Xu, Y. X.; Zhao, L.; Li, C.; Shi, G. Q. *Chem. Commun.* **2009**, *13*, 1667−1669.
(41) Hong, W.; Bai, H.; Xu, Y.; Yao, Z.; Gu, Z.; Shi, G. *J. Phys. Chem. C* **2010**, *114*, 1822−1826.
(42) Lu, J.; Do, I.; Drzal, L. T.; Worden, R. M.; Lee, I. *ACS Nano* **2008**, *2*, 1825−1832.
(43) Sun, C. L.; Lee, H. H.; Yang, J. M.; Wu, C. C. *Biosens. Bioelectron.* **2011**, *26*, 3450−3455.
(44) Yue, Q. L.; Zhang, K.; Chen, X. M.; Wang, L.; Zhao, J. S.; Liu, J. F.; Jia, J. B. *Chem. Commun.* **2010**, *46*, 3369−3371.
(45) Shen, J. F.; Shi, M.; Li, N.; Yan, B.; Ma, H. W.; Hu, Y. Z.; Ye, M. X. *Nano Res.* **2010**, *3*, 339−349.
(46) Goncalves, G.; Marques, P. A. A. P.; Granadeiro, C. M.; Nogueira, H. I. S.; Singh, M. K.; Grácio, J. *Chem. Mater.* **2009**, *21*, 4796−4802.
(47) Liu, J. B.; Li, Y. L.; Li, Y. M.; Li, J. H.; Deng, Z. X. *J. Mater.Chem.* **2010**, *20*, 900−906.
(48) Quintana, M.; Spyrou, K.; Grzelczak, M.; Browne, W. R.; Rudolf, P.; Prato, M. *ACS Nano* **2010**, *4*, 3527−3533.
(49) Kim, Y. K.; Na, H. K.; Min, D. H. *Langmuir* **2010**, *26*, 13065−13070.
(50) Muszynski, R.; Seger, B.; Kamat, P. V. *J. Phys. Chem. C* **2008**, *112*, 5263−5266.
(51) Hummers, W. S.; Offeman, R. E. *J. Am. Chem. Soc.* **1958**, *80*, 1339−1339.
(52) Jana, N.R.; Gearheart, L.; Murphy, C. J. *Langmuir* **2001**, *17*, 6782−6786.
(53) Nakamoto, K. *Infrared and Raman Spectra of Inorganic and Coordination Compounds*, 4th ed.; John Wiley & Sons: New York, 1986.
(54) Zhou, J.; Chen, M.; Diao, G, W. *J. Mater. Chem. A* **2013**, *1*, 2278−2285.
(55) Zhou, J.; Chen, M.; Diao, G, W. *ACS Appl. Mater. Interfaces* **2013**, *5*, 828−836.
(56) Han, C.; Ma, F.; Zhang, Z.; Xia, B.; Yu, Y.; Huang, F. *Org Lett.* **2010**, *12*, 4360−4363.
(57) Carrillo-Carrión, C.; Lendl, B.; Simonet, B. M.; Valcárcel, M. *Anal. Chem.* **2011**, *83*, 8093−8100.
(58) Sayin, S.; Yilmaz, M.; Tavasli, M. *Tetrahedron* **2011**, *67*, 3743−3753.
(59) Chen, M.; Diao, G. W. *J. Solution Chem.* **2011**, *40*, 481−491.
(60) Liu, Y.; Han, B. H.; Chen, Y. T. *J. Phys. Chem. B* **2002**, *106*, 4678−4687.
(61) Guo, Y.; Guo, S.; Li, J.; Wang, E.; Dong, S. *Talanta* **2011**, *84*, 60−64.
(62) Xu, C.; Wang, J.; Wan, L.; Lin, J.; Wang, X. *J. Mater. Chem.* **2011**, *21*, 10463−10471.
(63) Guo, Y.; Guo, S.; Ren, J.; Zhai, Y.; Dong, S.; Wang, E. *ACS Nano* **2010**, *4*, 4001−4010.
(64) Dursun, Z.; Gelmez, B. *Electroanalysis* **2010**, *22*, 1106−1114.
(65) Huang, J. S.; Liu, Y.; Hou, H. Q.; You, T. Y. *Biosens. Bioelectron.* **2008**, *24*, 632−637.
(66) Han, D.; Han, T.; Shan, C.; Ivaska, A.; Niu, L. *Electroanalysis* **2010**, *22*, 2001−2008.
(67) Alarcon-Angeles, G.; Perez-Lopez, B.; Palomar-Pardave, M.; Ramirez-Silva, M. T.; Alegret, S.; Merkoci, A. *Carbon* **2008**, *46*, 898−906.